



Structural incorporation of europium into uranium oxides

Shannon Kimberly Potts¹ · Philip Kegler¹ · Giuseppe Modolo¹ · Martina Klinkenberg¹ · Simon Hammerich² · Irmgard Niemeyer¹ · Dirk Bosbach¹ · Stefan Neumeier¹

Received: 10 January 2023 / Accepted: 7 February 2023 / Published online: 2 March 2023
© The Author(s) 2023

Abstract

Microparticulate reference materials with well-defined properties are needed by the International Atomic Energy Agency (IAEA) to consolidate a sustainable quality control system for analytical measurements for particle analysis in nuclear safeguards. In order to further develop analytical methods and quality control of the analytical results from particle analysis to detect even traces of dopants, such as fission products, the microparticulate reference materials must be refined according to the IAEA's requirements. Due to yield limitations of the microparticles, a co-precipitation method was adapted to synthesize bulk-scale comparison materials doped with lanthanides to unravel the incorporation mechanism of those dopants into the uranium oxide structure in depth. Through TG-DSC studies, the temperature range of phase transitions from UO_3 to U_3O_8 was identified and analyzed in more detail by additional systematic structural investigations of long- and short-range order phenomena with XRD and Raman, and IR, respectively.

Introduction

For the Quality Assurance and Control (QA/QC) system of analytical measurements on so-called environmental samples and particularly the U-containing microparticles, which are collected by IAEA safeguards inspectors during in-field verification, the IAEA needs microparticulate reference materials [1]. These reference microparticles must fulfill certain requirements, such as a well-defined elemental and isotopic composition, size, morphology, and a certain shelf-life, including storability and chemical durability over a certain period of time, to implement a robust QC system for the particle analysis of these environmental swipe samples in order to evaluate the absence of undeclared nuclear materials and activities [1]. Therefore, a physical aerosol-based method was implemented in the safeguards laboratories at Forschungszentrum Jülich to provide such microparticulate reference materials to the IAEA according to their requirements. Nowadays, these activities led to two successfully

certified batches of pure microparticulate uranium oxide reference materials [2, 3].

Additionally, the IAEA is also requesting doped uranium oxide microparticles as reference materials for method development of mass spectrometric analytical methods, such as Large Geometry-Secondary Ion Mass Spectrometry (LG-SIMS) to even detect traces of fission products, for instance and consequently, to increase the sensitivity of the mass spectrometric method and to identify challenges linked to the existence of, e.g., isobaric interferences during LG-SIMS measurements. Therefore, the uranium oxide reference materials must be further developed in the direction of composite (U-lanthanides, U-Th, and U-Pu) reference materials in microparticulate form [4]. First attempts in this direction were already performed by doping uranium oxide microparticles with neodymium and thorium [4, 5]. To enable the production of microparticles with a homogenous distribution of the dopant in the uranium oxide matrix of the microparticle and the prediction about the chemical stability of these microparticles, material science aspects such as the crystal structure and consequently the incorporation mechanism of the dopant into the uranium oxide structure must be investigated. However, due to the quantity limitation of the aerosol-based set-up in Jülich to produce these reference microparticles, structural investigations are very challenging and mainly limited to synchrotron experiments. Therefore, a synthesis route was adapted to produce ammonium diuranate

✉ Shannon Kimberly Potts
s.potts@fz-juelich.de

¹ Forschungszentrum Jülich GmbH, Institute of Energy and Climate Research – Nuclear Waste Management (IEK-6), 52425 Jülich, Germany

² Institute of Earth Sciences, Heidelberg University, 69120 Heidelberg, Germany

(ADU) doped with lanthanides (*Ln*'s) and Th as a sort of “internal reference materials”, which serve as a bulky model system for the microparticulate material that can be investigated with state-of-the-art analytical laboratory techniques. First, these internal reference materials were investigated with thermogravimetric analyses and differential scanning calorimetry (TG-DSC) to identify the temperature ranges at which the phase transformation to U_3O_8 occurs. In the second step, the materials were calcined at specific temperatures derived from the TG-DSC results to investigate the structural incorporation of the dopants into the uranium oxide structure and finally, to transfer these findings to the microparticulate system [6]. This paper discusses exemplarily the several steps of investigation by means of undoped uranium materials and 10 mol% Eu-doped uranium materials and provides for the first time insight into the structural incorporation of a lanthanide into UO_3 and U_3O_8 . Eu was chosen because its ionic radius lies exactly in the middle of the *Ln*'s series.

Materials and methods

Within this work, no experiments on human and animal subjects are reported.

Synthesis of the un- and 10 mol% Eu-doped ammonium diuranate, $(\text{NH}_4)_2\text{U}_2\text{O}_7$

The synthesis of ADU $(\text{NH}_4)_2\text{U}_2\text{O}_7$ without and with Eu as dopant was performed using an aqueous solution of uranyl nitrate $(\text{UO}_2(\text{NO}_3)_2 \cdot 6 \text{H}_2\text{O})$ for the undoped ADU and an aqueous mixed solution of uranyl and europium nitrate $(\text{Eu}(\text{NO}_3)_3 \cdot 6 \text{H}_2\text{O})$ (99.99%, Alfa Aesar) for the 10 mol% Eu-doped ADU. The prepared solutions were slowly added to an excess of at least 300% ammonia ($w(\text{NH}_3) = 32\%$; Merck KGaA) while stirring. The resulting precipitates were stirred for 2 h to ensure a complete precipitation. The synthesized materials were washed several times with MilliQ® water and finally elutriated with ethanol and dried. More detailed information was published by Potts et al. [6].

Characterization of the internal reference material

Thermogravimetric analyses and differential scanning calorimetry (TG-DSC)

The previously synthesized materials were analyzed using thermogravimetric analyses and differential scanning calorimetry (TG-DSC). For this purpose, a NETZSCH STA 449 F1 Jupiter was used, which was operated using Pt/Rh

crucibles and a heating rate of $10 \text{ K} \cdot \text{min}^{-1}$ in synthetic air (80/20).

Scanning electron microscopy—energy-dispersive X-ray spectroscopy (SEM-EDX), X-ray diffraction (XRD), Raman-, and Infrared spectroscopy (IR)

Based on the TG-DSC measurements, the temperatures 520 °C, 700 °C, and 1200 °C were identified for calcination. The un- and Eu-doped materials were calcined in air for 5 h using the CARBOLITE CWF 1300 chamber furnace.

The chemical composition of the un- and 10 mol% Eu-doped materials calcined at 520 °C, 700 °C, and 1200 °C was investigated by using a FEI Quanta 200F environmental scanning electron microscope equipped with an energy-dispersive X-ray spectrometer (EDAX) operated in low vacuum modus (60 Pa) at 20 kV. Therefore, the calcined powders were placed on SEM specimen stubs with carbon adhesive discs without pretreatment (e.g., pestling). X-ray diffraction (XRD) patterns of the materials after calcination were recorded by means of a Bruker D4 Endeavor diffractometer equipped with a *1D* Lynx-eye detector in Bragg–Brentano configuration using $\text{CuK}_{\alpha 1,2}$ radiation ($\lambda = 1.54184 \text{ \AA}$). XRD data were collected at room temperature in the $10^\circ \leq 2\theta \leq 120^\circ$ range with a step size of $(2\theta) = 0.01^\circ$ and a counting time of 2 s per step.

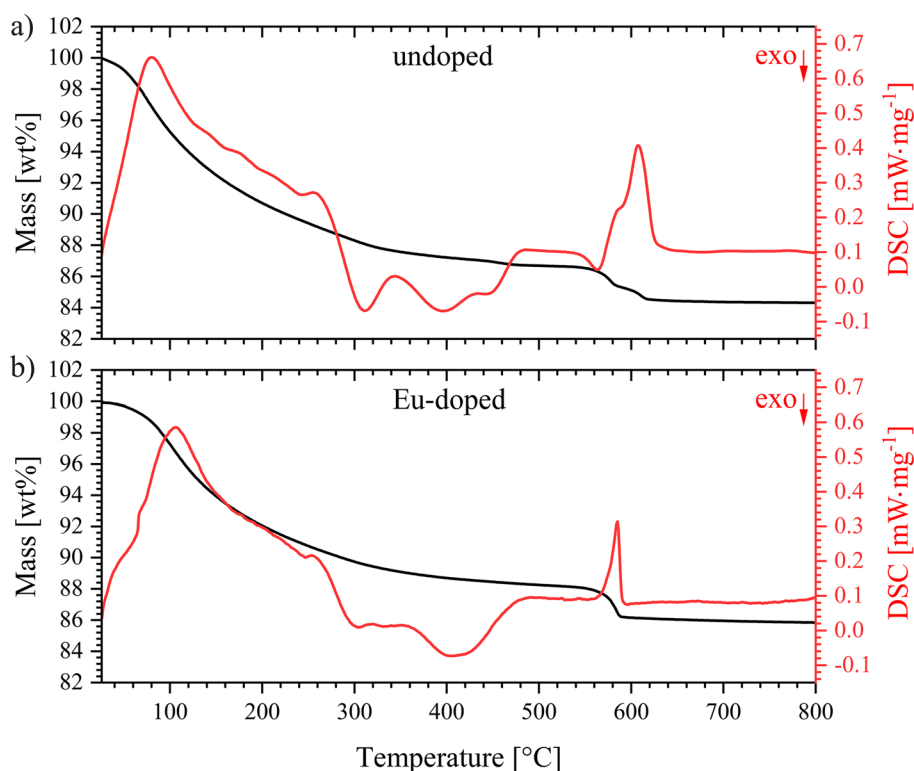
The Raman spectra of all materials were collected using a Horiba LabRAM HR spectrometer with a Peltier-cooled multichannel CCD detector. Therefore, small quantities of the calcined powder had to be pressed into pellets. The Raman spectra of the compounds were recorded at room temperature in the range of 100 cm^{-1} to 1000 cm^{-1} using a He–Ne laser at a power of 17 mW ($\lambda = 632.8 \text{ nm}$). The spectral resolution was around 1 cm^{-1} with a slit of $100 \mu\text{m}$.

Infrared (IR) spectroscopy of KBr pellets was done using a Bruker Invenio-R infrared spectrometer with a resolution of 4 cm^{-1} and 32 scans per sample.

Results and discussion

The synthesized internal reference materials—the undoped ammonium diuranate (ADU) and 10 mol% Eu-doped ADU sample—were investigated to understand the influence of the dopant on the formation of the uranium oxide structures using state-of-the-art analytical methods. The selected doping level of 10 mol% Eu was chosen to guarantee either detectability of Eu incorporation or segregation of Eu phases. To be able to describe the decomposition behavior and identify differences in the decomposition behavior caused by the dopant, TG-DSC measurements were carried out. The performed TG-DSC measurements for both samples are shown in Fig. 1. Figure 1a shows the

Fig. 1 TG-DSC measurements of **a** undoped ADU and **b** 10 mol% Eu-doped ADU performed in synthetic air



TG-DSC thermogram of the undoped ADU as a function of temperature. The thermal decomposition of the undoped ADU can be described in several steps which are in very good agreement to the existing literature. The initial mass loss and the endothermic DSC signal up to a temperature of 285 °C indicates the H_2O release and the subsequent exothermic DSC signals at 311 °C and 397 °C correspond to the removal of NH_3 according to the literature [7]. The additional exothermic DSC signal at 445 °C and the mass loss in the range of 428 °C to 500 °C with 0.38 wt% indicate the formation of a $\beta\text{-UO}_3$ phase [7]. The significant mass loss in the temperature ranges from 520 °C to 700 °C can be assigned to the formation of U_3O_8 . During this phase transformation to U_3O_8 , the TG signal shows a two-step mass loss. This indicates that a mixture of UO_3 and/or $\text{UO}_{2.9}$ and an amorphous phase is present [8, 9]. Some recent studies have addressed the characterization of the amorphous phase, reporting it to be either stoichiometric U_2O_7 [10], or an amorphous UO_3 hydrate [11]. Furthermore, the gradual decomposition of the amorphous phase, via the formation of the intermediate $\alpha\text{-UO}_{2.9}$ and finally the formation of the U_3O_8 phase, has been described in the literature [8, 9, 12]. This decomposition behavior can also be observed here in the TG of the undoped sample based on the plateau formed after the first mass loss step (~ 589 °C) and the mass loss of the second mass loss step of 0.92 wt% (591–700 °C). Both steps indicate the formation of an intermediate, such as $\alpha\text{-UO}_{2.9}$. This assumption is supported by the exothermic DSC

signal (565 °C) observed at the first mass loss step assigning to the crystallization of the amorphous phase. The following endothermic DSC signal (~ 584 °C) indicates a crystalline phase transition. At the second mass loss step, an endothermic DSC signal (610 °C) is evident, which overlaps with the previous endothermic DSC signal. These observations in the DSC support the assumption that a polymorphic mixture of $\beta\text{-UO}_3$, $\alpha\text{-UO}_3$ and/or $\alpha\text{-UO}_{2.9}$ and amorphous material is present, which is converted subsequently to U_3O_8 .

The influence of the Eu doping on the decomposition behavior of the ADU sample was analyzed applying the same TG-DSC protocol. The TG-DSC measurement of the Eu-doped sample is shown in Fig. 1b. The initial decomposition of the Eu-doped sample is very similar to the decomposition of the undoped sample with respect to the removal of water (280 °C) and NH_3 (around 305 °C and 406 °C). In contrast to the measurements of the undoped material, no indications of the formation of $\beta\text{-UO}_3$ could be identified. The endothermic DSC signal and the absence of a pronounced plateau in the temperature range from 520 °C to 700 °C assign to a phase transition without significant formation of the intermediate $\alpha\text{-UO}_{2.9}$. However, according to the literature, the rounded shape of the mass loss step could point to the presence of $\alpha\text{-UO}_3$ and/or $\alpha\text{-UO}_{2.9}$ with a portion of an amorphous phase [8]. The absence of the exothermic DSC signal at 565 °C in comparison to the undoped material could indicate that overlapping competing phase transitions are taking place here. After the phase transformation in the

temperature range from 520 °C to 620 °C, the material is present as U_3O_8 . The mass losses due to the formation of U_3O_8 in the temperature range from 520 °C to 700 °C are approximately the same for both materials (2.32 wt.% for undoped sample and 2.23 wt.% for Eu-doped sample). However, it can also be observed that the doping of the material shifts the region of the phase transition to U_3O_8 to a lower temperature range (temperature of the maximum of the endothermic DSC signal: 610 °C for undoped sample; 583 °C for Eu-doped sample). The endothermic reaction enthalpy ΔH_m for the formation of U_3O_8 decreases from 55.(5) $\text{kJ}\cdot\text{mol}^{-1}$ (undoped) to 15.(7) $\text{kJ}\cdot\text{mol}^{-1}$ (Eu-doped). These observations imply that Eu doping strongly affects the phase transformation from UO_3 to U_3O_8 .

In order to investigate the phase transformation to U_3O_8 in more detail, the undoped and Eu-doped samples were calcined at 520 °C before and at 700 °C after the phase transformation, based on the temperatures identified from TG-DSC measurements. To evaluate the chemical composition as well as the distribution of the dopant Eu after calcination at 520 °C, SEM-EDX mappings were performed. Fig. A1a (cf. SI) shows that Eu is homogeneously distributed with a fraction of 17.(2) at% Eu in the sample. Apparently, the measured value deviates from the expected Eu content. However, this measured value is indicative considering the error margin of the device and the initial weight and is within the tolerable range of the theoretically expected value of 10 mol% Eu. In addition, the undoped and Eu-doped materials were structurally investigated after calcination using XRD (Fig. 2a, b) and Raman spectroscopy (Fig. 2c).

A comparison of XRD patterns of the undoped material with the reference data indicate the formation of a phase mixture of $\alpha\text{-UO}_3$ [13], $\beta\text{-UO}_3$ [14], and an amorphous fraction after calcination at 520 °C (Fig. 2a), which corresponds to the literature [14, 15]. These findings largely agree with the interpretation of the TG-DSC measurement. The missing

reflexes of an $\alpha\text{-UO}_{2.9}$ phase do not imply the absence of an intermediate formation of $\alpha\text{-UO}_{2.9}$ at 520 °C, since the $\alpha\text{-UO}_{2.9}$ phase is instable at room temperature and re-oxidizes to $\alpha\text{-UO}_3$ [9]. The diffractogram of Eu-doped material after calcination at 520 °C shows the formation of a phase mixture of $\alpha\text{-UO}_3$, an amorphous phase, and traces of $\beta\text{-UO}_3$ at a 2θ value of 29° (Fig. 2b). These results support the observations of the TG-DSC measurement of the Eu-doped sample. The characteristics of the reflexes as well as the increased amorphous background indicate an amorphization of the sample caused by the dopant Eu. These conclusions are underpinned by the Raman spectrum of the Eu-doped sample (Fig. 2c) (blue)). The identified vibrations of the Eu-doped sample point to an amorphization of the sample, which has clear characteristics due to the diffuse and broad Raman band centered at 685 cm^{-1} with low-intensity shoulders at 755 cm^{-1} and 857 cm^{-1} [16]. On the contrary, the observed vibrations in the Raman spectrum of the undoped sample show vibrations which can be assigned to the UO_3 and amorphous phases (cf. SI, Table A1) [15, 17]. As a consequence, the XRD and Raman results prove that the amorphous phase was stabilized by the doping.

The influence of the dopant Eu after the phase transformation was studied after calcination at 700 °C using SEM-EDX and IR spectroscopy complementary to the previously published XRD and Raman investigations [6]. The SEM-EDX mapping (Fig. 3a) again demonstrates a constant homogeneous distribution of Eu with an indicatively measured fraction of 15.(0) at% Eu. In previous publications, it was already shown that doping with Eu stabilizes the hexagonal phase with the space group $P\bar{6}2m$, which is normally instable at temperatures below temperatures of 350 °C [6, 18]. However, the undoped sample showed the formation of the expected orthorhombic U_3O_8 phase with the space group $C2mm$. Considering the normalized volumes of $333.08(1)\text{ Å}^3$ (undoped) and $334.70(6)\text{ Å}^3$ (Eu-doped), a significant lattice expansion

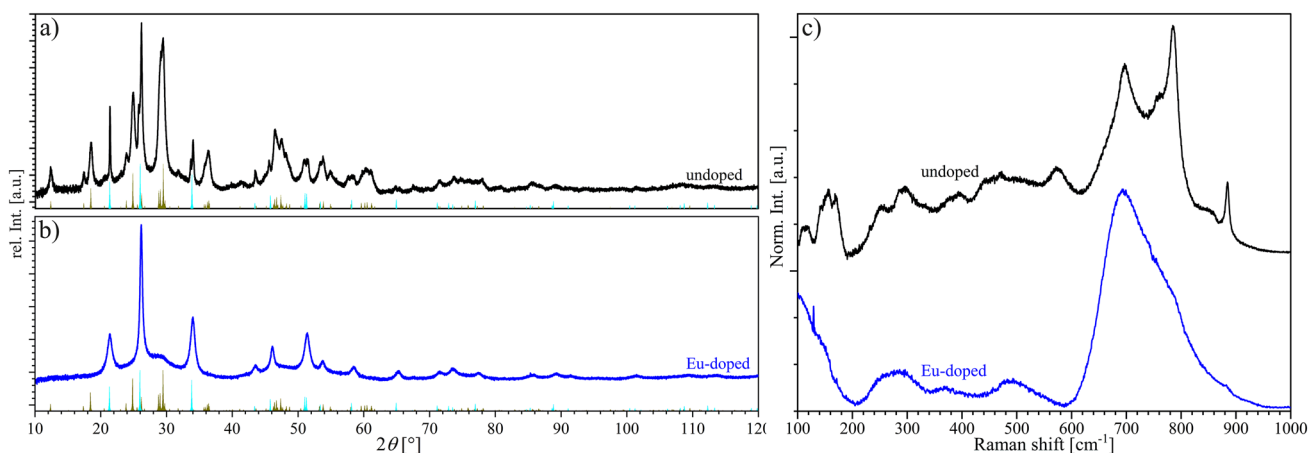


Fig. 2 XRD of the **a** undoped and **b** Eu-doped samples as well as **c** Raman spectra of the undoped (black) and Eu-doped (blue) samples after calcination at 520 °C (XRD References: $\alpha\text{-UO}_3$ with the space group $C2mm$ (cyan) [13]; $\beta\text{-UO}_3$ with the space group $P2_1$ (dark green) [14])

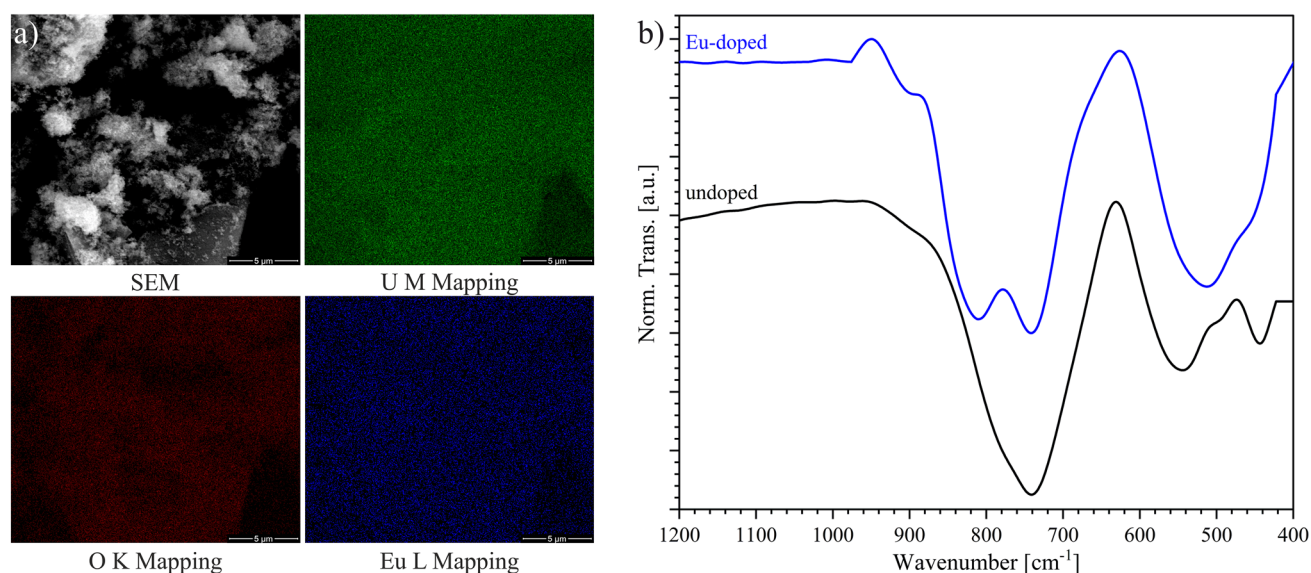


Fig. 3 **a** EDX mapping analysis of 10 mol% Eu-doped samples and **b** IR spectra of undoped U_3O_8 (black) and 10 mol% Eu-doped U_3O_8 (blue)

of the structure can be observed [6]. Since the Eu^{3+} -ion has a larger ionic radius ($r(\text{Eu}^{3+}) = 1.087 \text{ \AA}$ [19]) than uranium in the U_3O_8 structure ($r(\text{U}^{6+}) = 0.87 \text{ \AA}$; $r(\text{U}^{5+}) = 0.9 \text{ \AA}$ [19]), the volume expansion indicates the Eu substitution at the U^{5+} site [6, 20]. Complementary to the already published findings, infrared spectroscopic measurements were conducted. Figure 3b shows the IR spectra of the undoped and Eu-doped samples after calcination at 700 °C. The IR spectrum of the undoped sample shows U–O stretching vibration modes at 444 cm^{-1} , 496 cm^{-1} , 548 cm^{-1} , and 743 cm^{-1} that can be assigned to orthorhombic U_3O_8 [21, 22]. The IR spectrum of the Eu-doped sample shows differences compared to the IR spectrum of the undoped sample. According to the literature, the U–O stretching vibrations at 455 cm^{-1} , 513 cm^{-1} , 742 cm^{-1} , and 810 cm^{-1} can be assigned to the hexagonal U_3O_8 (cf. SI, Table A2) [21]. An additional vibrational mode around the wavenumber 890 cm^{-1} indicates the anti-symmetric stretching uranyl vibration (980–830 cm^{-1}), which could be caused by the presence of a uranyl bond in the Eu-doped sample as a consequence of the Eu incorporation into the U_3O_8 structure [17, 23]. This also supports the assumption that there is a hexagonal U_3O_8 structure ($P6_2m$) in the doped material, which shows local distortions due to uranyl units similar to the structural model developed by Caisso et al. [20]. No vibrations in the IR spectrum could be ascribed to Eu_2O_3 [24]. The results from previously published investigations [6] as well as the additional IR investigations in this study demonstrate that the dopant Eu can be incorporated into the U_3O_8 structure.

The structural incorporation of Ln's into a hexagonal U_3O_8 structure is not described in the literature so far. Bernt et al. [25] described a phase separation, which consists of

an orthorhombic $\beta\text{-U}_3\text{O}_8$ phase and an Eu-rich cubic phase. However, the phase diagram was obtained at a temperature of 1250 °C. Therefore, the samples were calcined at 1200 °C and examined. The SEM image (cf. SI, Fig. A1b), top right) shows two different morphologies in the Eu-doped sample after calcination at 1200 °C, which consist of partly sintered microstructure with defined grain boundaries and individual particles. The SEM–EDX mappings (cf. SI, Fig. A1b)) instead show the expected homogeneous distribution of the dopant Eu in the material due to the spatial resolution of this technique, the volume probed as well as the size of the grains and crystallites formed. From XRD patterns, the formation of a phase mixture of $\alpha\text{-U}_3\text{O}_8$ and a cubic phase can be deduced. The formation of $\alpha\text{-U}_3\text{O}_8$ instead of the $\beta\text{-U}_3\text{O}_8$ expected from the phase diagram is caused by the fact that the $\beta\text{-U}_3\text{O}_8$ phase is only synthesized after heating $\alpha\text{-U}_3\text{O}_8$ at high temperatures with an additional slow cooling rate of 100 °C per day [26]. Since a different procedure for the preparation of the materials was applied in this study, the $\alpha\text{-U}_3\text{O}_8$ phase formed during the cooling. The reflex pattern of the cubic phase (marked in Fig. 4b)) could indicate the formation of a cubic Eu_2O_3 phase (space group $Ia\bar{3}$) [27] or the formation of a cubic Eu-rich uranium oxide phase similar to the observation of Dueber et al. [28] on the formation of a segregated cubic Mg-rich $\text{UO}_{2\pm x}$ phase besides a pure U_3O_8 phase starting from Mg-doped U_3O_8 using galvanometric discharging.

Complementary collected Raman spectra of the un- and Eu-doped samples (Fig. 4 c)) show vibrations of the U_3O_8 phase and no indication of the formation of a Eu_2O_3 phase (cf. SI, Table A3) [24, 29]. However, no bands are explicitly assigned to vibrations of the pure UO_2 phase (445 cm^{-1}) [30]

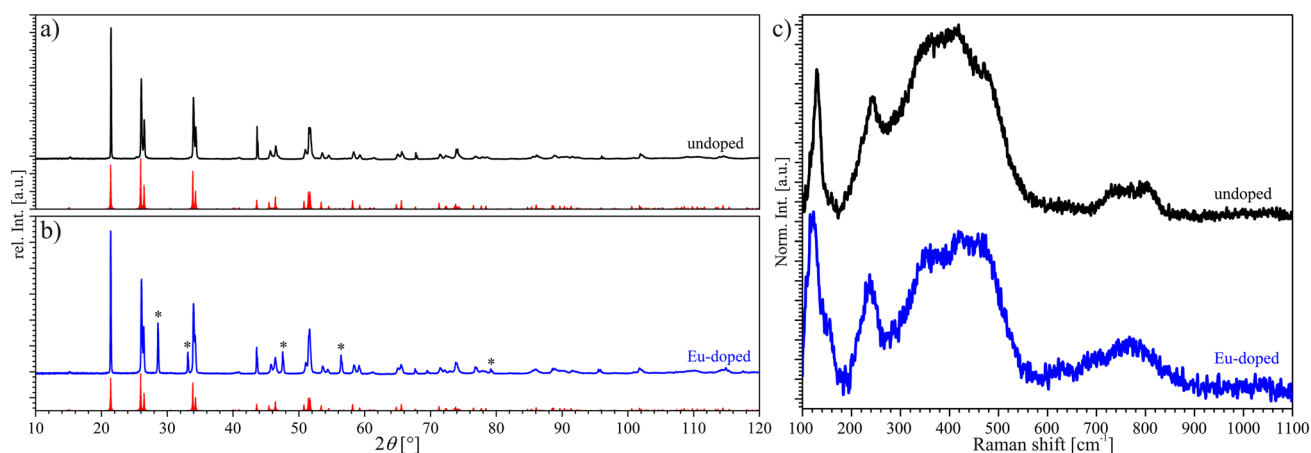
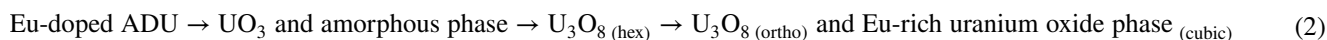
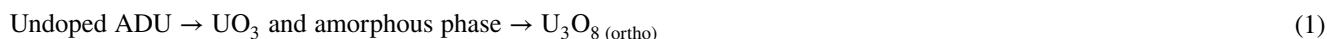


Fig. 4 XRD of the **a** undoped and **b** Eu-doped samples as well as **c** Raman spectra of the undoped (black) and Eu-doped (blue) samples after calcination at 1200 °C (XRD Reference: α - U_3O_8 with the space group $C2mm$ (red) [18])

or the doped UO_2 phase, which shows according to the literature [31] a splitting of the intense band at 445 cm^{-1} into two low-intensity bands (450 cm^{-1} and broad band between 500 cm^{-1} and 700 cm^{-1}) after doping UO_2 with Gd and leads to a defect structure of the U_4O_9 phase. Since these weak bands are highly laser sensitive, it is possible that the bands cannot be measured with a laser using the wavelength 633 nm or are so weak that they are overlaid by the U_3O_8 bands.

Conclusion

The structural response of uranium oxide materials on Eu incorporation was investigated as an example for the Ln -doped uranium oxide system. It has been shown that doping ADU with a foreign ion (Eu^{3+}) affects the decomposition and phase transition to differ from that of the undoped material by lowering the phase transition temperature and reaction enthalpy ΔH_m . In addition, it was demonstrated that the doping leads to a stabilization of the amorphous phase at 520 °C (before phase transformation) as well as of the hexagonal U_3O_8 phase at higher temperatures (700 °C , after phase transformation). The measurements indicate that the dopant Eu can be incorporated into the uranium oxide structures without the evidence of the formation of a phase segregation of Eu_2O_3 . In general, the decomposition behavior of the undoped (1) as well as the Eu-doped (2) ADU proceeds according to the following ex situ schemes:



Supplementary Information The online version contains supplementary material available at <https://doi.org/10.1557/s43580-023-00522-4>.

Acknowledgments This publication was prepared as an account of work within the Joint Programme on the Technical Development and Further Improvement of IAEA Safeguards between the Federal Ministry for the Environment, Nature Conservation, Nuclear Safety and Consumer Protection, Germany under Task C45/A1961, and the IAEA. We acknowledge Z. Paparigas, M. Güngör, and N. Lieck from Forschungszentrum Jülich GmbH for experimental and analytical support. The datasets generated during and/or analyzed during the current study are available from the corresponding author on reasonable request.

Funding Open Access funding enabled and organized by Projekt DEAL. Funding was provided by Bundesministerium für Umwelt, Naturschutz, nukleare Sicherheit, und Verbraucherschutz (C45/A1961).

Declarations

Conflict of interest On behalf of all authors, the corresponding author states that there is no conflict of interest.

Open Access This article is licensed under a Creative Commons Attribution 4.0 International License, which permits use, sharing, adaptation, distribution and reproduction in any medium or format, as long as you give appropriate credit to the original author(s) and the source, provide a link to the Creative Commons licence, and indicate if changes were made. The images or other third party material in this article are included in the article's Creative Commons licence, unless indicated otherwise in a credit line to the material. If material is not included in the article's Creative Commons licence and your intended use is not permitted by statutory regulation or exceeds the permitted use, you will

need to obtain permission directly from the copyright holder. To view a copy of this licence, visit <http://creativecommons.org/licenses/by/4.0/>.

References

1. K.G.W. Inn, C.M. Johnson, W. Oldham, S. Jerome, L. Tandon, T. Schaaff, R. Jones, D. Mackney, P. MacKill, B. Palmer, D. Smith, S. LaMont, J. Griggs, J. Radioanal. Nucl. Chem. **296**, 5 (2012)
2. J. Truyens, M. Dürr, Z. Macsik, R. Middendorp, S. Neumeier, S. Richter, G. Stadelmann, C. Venchiarutti, Y. Aregbe, *EUR29840* (Publications Office of the European Union, Luxembourg, 2020)
3. J. Truyens, S. Neumeier, P. Kegler, M. Klinkenberg, M. Zoriy, S. Richter, Y. Aregbe, *EUR30625* (Publications Office of the European Union, Luxembourg, 2021)
4. P. Kegler, F. Pointurier, J. Rothe, K. Dardenne, T. Vitova, A. Beck, S. Hammerich, S. Potts, A.-L. Faure, M. Klinkenberg, MRS Adv. **6**, 125 (2021)
5. P. Asplanato, W. Zannouh, A.L. Fauré, P.H. Imbert, J. Lautru, M. Cornaton, N. Dacheux, F. Pointurier, N. Clavier, J. Nucl. Mater. **573**, 154142 (2023)
6. S.K. Potts, P. Kegler, G. Modolo, S. Hammerich, I. Niemeyer, D. Bosbach, S. Neumeier, MRS Adv. **7**, 128 (2022)
7. C. Schreinemachers, G. Leinders, G. Modolo, M. Verwerft, K. Binnemans, T. Cardinaels, Nucl. Eng. Technol. **52**, 1013 (2020)
8. H.R. Hoekstra, S. Siegel, J. Inorg. Nucl. Chem. **18**, 154 (1961)
9. R. Thomas, M. Rivenet, E. Berrier, I. de Waele, M. Arab, D. Amaraggi, B. Morel, F. Abraham, J. Nucl. Mater. **483**, 149 (2017)
10. S.O. Odoh, J. Shamblin, C.A. Colla, S. Hickam, H.L. Lobeck, R.A. Lopez, T. Olds, J.E. Szymanowski, G.E. Sigmon, J. Neufeind, W.H. Casey, M. Lang, L. Gagliardi, P.C. Burns, Inorg. Chem. **55**, 3541 (2016)
11. X. Guo, S.V. Ushakov, S. Labs, H. Curtius, D. Bosbach, A. Navrotsky, Proc. Natl. Acad. Sci. USA **111**, 17737 (2014)
12. L. Desfougeres, E. Welcomme, M. Ollivier, P.M. Martin, J. Hen-nuyer, M. Hunault, R. Podor, N. Clavier, L. Favergeon, Inorg. Chem. **59**, 8589 (2020)
13. B.O. Loopstra, E.H.P. Cordfunke, Recl. Trav. Chim. Pays-Bas **85**, 135 (1966)
14. P. Debets, Acta Cryst. **21**, 589 (1966)
15. N.B.A. Thompson, V.L. Frankland, J.W.G. Bright, D. Read, M.R. Gilbert, M.C. Stennett, N.C. Hyatt, J. Radioanal. Nucl. Chem. **327**, 1335 (2021)
16. T.G. Ditcham, A. Wotherspoon, K.P. Kirkbride, C.E. Lenehan, R.S. Popelka-Filcoff, J. Radioanal. Nucl. Chem. **310**, 725 (2016)
17. T.L. Spano, A.E. Shields, B.S. Barth, J.D. Gruidl, J.L. Niedziela, R.J. Kapsimalis, A. Miskowicz, Inorg. Chem. **59**, 11481 (2020)
18. R. Ackermann, A. Chang, C.A. Sorrell, J. Inorg. Nucl. Chem. **39**, 75 (1977)
19. R.D. Shannon, Acta Cryst. **A32**, 751 (1976)
20. M. Caisso, P. Roussel, C. Den Auwer, S. Picart, C. Hennig, A.C. Scheinost, T. Delahaye, A. Ayral, Inorg. Chem. **55**, 10438 (2016)
21. G. Socrates, *Infrared and Raman Characteristic Group Frequencies: Tables and Charts*, 3rd edn. (Wiley, Chichester, 2004), pp.323–325
22. S. Siegel, H.R. Hoekstra, Inorg. Nucl. Chem. Lett. **7**, 497 (1971)
23. G. Lu, A.J. Haes, T.Z. Forbes, Coord. Chem. Rev. **374**, 314 (2018)
24. M.W. Urban, B.C. Cornilsen, J. Phys. Chem. Solids **48**, 475 (1987)
25. U. Berndt, R. Tanamas, C. Keller, J. Solid State Chem. **17**, 113 (1976)
26. A. Miskowicz, T. Spano, R. Hunt, J.M. Kurley, J. Nucl. Mater. **568**, 153894 (2022)
27. V. Katari, S.N. Achary, S.K. Deshpande, P.D. Babu, A.K. Sinha, H.G. Salunke, N. Gupta, A.K. Tyagi, J. Phys. Chem. C. **118**, 17900 (2014)
28. R.E. Dueber, J.M. Fleetwood, P.G. Dickens, Solid State Ion. **50**, 329 (1992)
29. S.D. Senanayake, R. Rousseau, D. Colegrave, H. Idriss, J. Nucl. Mater. **342**, 179 (2005)
30. L. Desgranges, G. Baldinozzi, P. Simon, G. Guimbretière, A. Canizares, J. Raman Spectrosc. **43**, 455 (2012)
31. M. Razdan, D.W. Shoesmith, J. Electrochem. Soc. **161**, H105 (2013)

Publisher's Note Springer Nature remains neutral with regard to jurisdictional claims in published maps and institutional affiliations.